Lipid-based Nanoparticle Delivery of Pre-miR-107 Inhibits the Tumorigenicity of Head and Neck Squamous Cell Carcinoma

Longzhu Piao[1,2], Manchao Zhang[1,2], Jharna Datta[1,2], Xiujie Xie[1,2], Tizhi Su[1,2], Hong Li[3], Theodoros N Teknos[1,2] and Quintin Pan[1,2]

[1]Department of Otolaryngology-Head and Neck Surgery, The Ohio State University Medical Center, Columbus, Ohio, USA; [2]Arthur G. James Cancer Hospital and Richard J. Solove Research Institute, The Ohio State University Comprehensive Cancer Center, Columbus, Ohio, USA; [3]Division of Pharmaceutics, College of Pharmacy, The Ohio State University, Columbus, Ohio, USA

Head and neck squamous cell carcinoma (HNSCC) is the sixth most prevalent cancer worldwide with about 600,000 new cases diagnosed in the last year. Our laboratory showed that miR-107 expression is reduced and functions as a tumor suppressor gene in HNSCC suggesting the potential application of miR-107 as a novel anticancer therapeutic. In this study, we determined the efficiency and efficacy of cationic lipid nanoparticles to deliver pre-miR-107 (NP/pre-miR-107) in HNSCC cells *in vitro* and *in vivo*. NP/pre-miR-107 increased delivery of miR-107 into HNSCC cells by greater than 80,000-fold compared to free pre-miR-107. Levels of known miR-107 targets, protein kinase Cε (PKCε), cyclin-dependent kinase 6 (CDK6), and hypoxia-inducible factor 1-β (HIF1-β), decreased following NP/pre-miR-107 treatment. Clonogenic survival, cell invasion, and cell migration of HNSCC cells was inhibited with NP/pre-miR-107. Moreover, NP/pre-miR-107 reduced the cancer-initiating cell (CIC) population and dampened the expression of the core embryonic stem cell transcription factors, Nanog, Oct3/4, and Sox2. In a preclinical mouse model of HNSCC, systemic administration of NP/pre-miR-107 significantly retarded tumor growth by 45.2% compared to NP/pre-miR-control ($P < 0.005$, $n = 7$). Kaplan–Meier analysis showed a survival advantage for the NP/pre-miR-107 treatment group ($P = 0.017$). Our results demonstrate that cationic lipid nanoparticles are an effective carrier approach to deliver therapeutic miRs to HNSCC.

Received 31 August 2011; accepted 11 March 2012; advance online publication 10 April 2012. doi:10.1038/mt.2012.67

INTRODUCTION

Approximately 600,000 new cases of head and neck squamous cell carcinoma (HNSCC) are diagnosed worldwide each year.[1,2] Most HNSCC patients present with locally advanced disease that requires a multi-disciplinary approach involving surgery, radiation, and chemotherapy. In spite of aggressive definitive treatment, patients with locally advanced HNSCC frequently develop locoregional recurrence and/or distant metastasis. The 5-year survival rate for HNSCC patients has remained static at around 50% over the past several decades. There remains a critical need to identify genetic alterations in HNSCC responsible for disease recurrence and metastasis to allow for better clinical management.

microRNAs (miRs) are short, 20–25 nucleotides, single-stranded noncoding RNAs that negatively regulate target protein levels by suppressing messenger RNA (mRNA) translation and/or enhancing mRNA degradation.[3] There is accumulating literature demonstrating that miRs may play a causative role in the development and/or progression of numerous cancers, including HNSCC.[4–8] In HNSCC, global miR expression analysis showed that miR-107 was significantly downregulated in primary tumors compared to matched normal tissue.[9] Furthermore, miR expression profiling of HNSCC cell lines and normal keratinocytes indicate that miR-107 expression is decreased at high frequency in HNSCC.[10] Recent work from our laboratory showed that a majority of HNSCC patients have reduced miR-107 expression in the primary tumor providing additional support that loss of miR-107 is a frequent event in the development of HNSCC.[11] In addition, ectopic expression of miR-107 is sufficient to dampen the tumorigenic potential of HNSCC cells *in vitro* and *in vivo*.[11] Our results indicate that reduction in miR-107 expression is a pathogenetic event in HNSCC and moreover, miR-107 may be used as an anticancer therapeutic for this patient population.[11]

The application of miRs as therapeutic agents in cancer is beginning to emerge. Systemic delivery of miRs remains a major obstacle due to inefficient uptake into target cells and degradation in circulation. In this study, we formulated cationic lipid nanoparticles as a carrier to protect and transport pre-miR-107 into HNSCC cells. Delivery of pre-miR-107 into HNSCC cells was dramatically enhanced with NP/pre-miR-107 compared to free pre-miR-107 or NP/pre-miR-control. Confirmed miR-107 target genes, protein kinase Cε (PKCε), hypoxia-inducible factor 1-β (HIF1-β), and cyclin-dependent kinase 6 (CDK6) were reduced in response to NP/pre-miR-107 treatment. CAL27 and UMSCC74A cells treated with NP/pre-miR-107 showed a marked reduction in cell invasion, cell migration, clonogenic survival, and tumorsphere formation. Importantly, intravenous administration of NP/miR-107 significantly retarded the tumor growth and

Correspondence: *Quintin Pan, Department of Otolaryngology-Head and Neck Surgery, The Ohio State University Medical Center, 442 Tzagournis Medical Research, 420 West 12th Avenue, Columbus, Ohio 43210, USA. E-mail: Quintin.Pan@osumc.edu*

extended the survival of nude mice bearing HNSCC xenografts. Our work indicates that cationic lipid nanoparticles are an effective approach to systemically deliver therapeutic miRs.

RESULTS

Nanoparticle encapsulation enhances the delivery of pre-miR-107 into HNSCC cells

Cationic lipid nanoparticles were prepared with dimethyldioctadecyl ammonium bromide (DDAB), cholesterol, and α-Tocopheryl polyethylene glycol 1000 succinate (TPGS) (molar ratio of 60:35:5) using the ethanol injection method. In **Figure 1a**, a representative transmission electron microscopy (TEM) image showed that the nanoparticles formulated were spherical in shape with a mean diameter of 150.1 ± 3.5 nm. The zeta potential was +10.3 ± 0.4 mV and the encapsulation efficiency of pre-miR-107 was 98.9 ± 1.5%. To determine the efficiency of the nanoparticle to deliver pre-miRs into HNSCC cells *in vitro*, HNSCC cells were untreated or treated with free FAM-labeled pre-miR-control or nanoparticle encapsulated FAM-labeled pre-miR-control (NP/FAM-pre-miR-control, 30 nmol/l for 24 hours) followed by fluorescence-activated cell sorting analysis (**Figure 1c**). HNSCC cell lines, SCC15, SCC25, CAL27, and UMSCC74A, treated with free FAM-labeled pre-miR-control resulted in 1.0, 1.6, 2.2, and 1.1% FAM-positive cells with a mean fluorescence intensity of 7.1, 6.3, 9.4, and 5.5, respectively. In contrast, NP/FAM-labeled pre-miR-control treatment resulted in 57.5% FAM-positive cells in SCC15, 63.3% FAM-positive cells in SCC25, 83.0% FAM-positive cells in CAL27, and 91.5% FAM-positive cells in UMSCC74A. The mean fluorescence intensity was 95.4 for SCC15 cells, 56.3 for

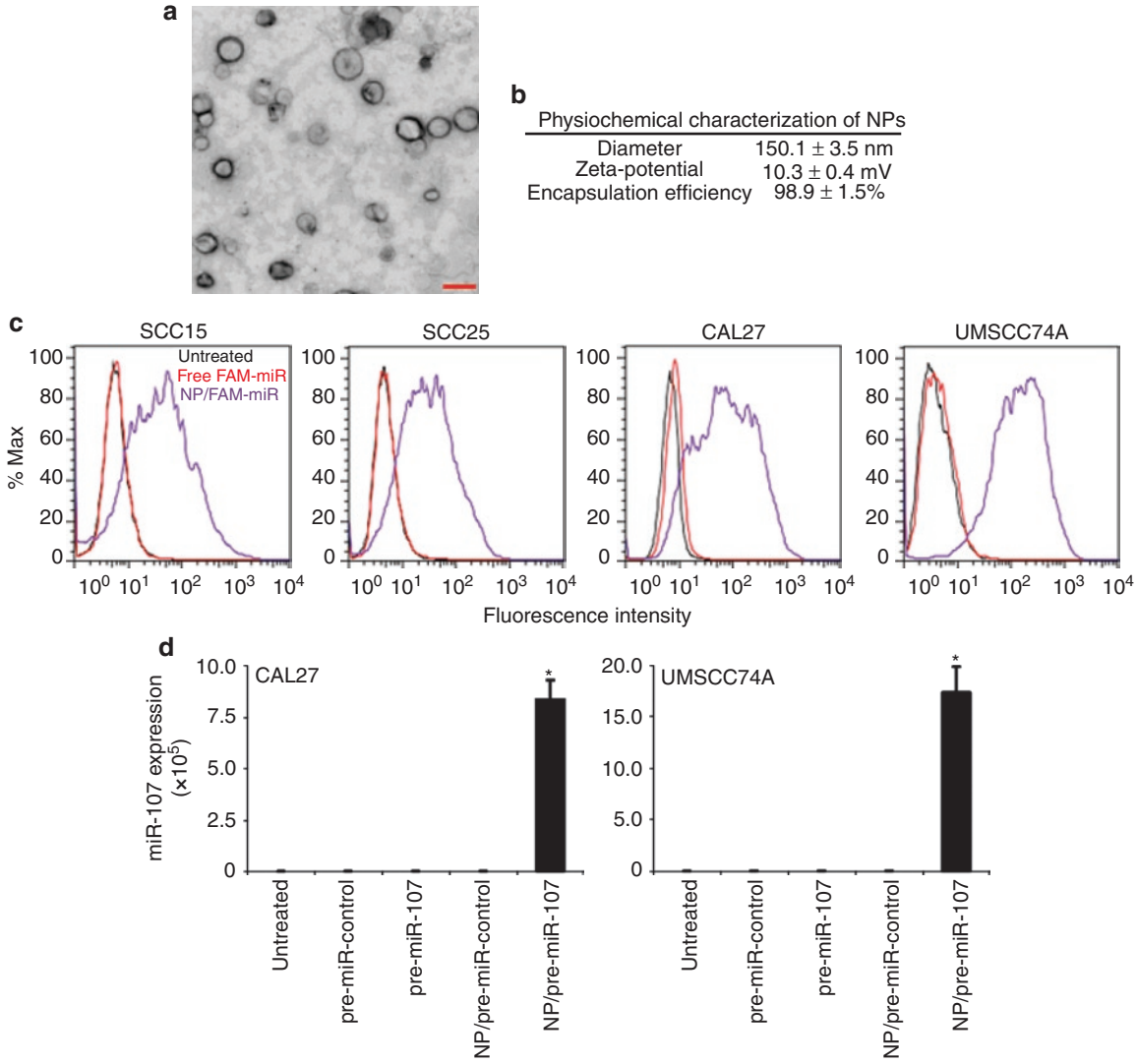

Figure 1 Nanoparticle encapsulation enhances the delivery of pre-miR-107 into HNSCC cells. (**a**) Transmission electron microscopy of cationic lipid nanoparticle. Bar = 200 nm. (**b**) Physiochemical properties of the cationic lipid nanoparticle. (**c**) Fluorescence-activated cell sorting (FACS) analysis of HNSCC cells. HNSCC cells were untreated or treated with 30 nmol/l of free or nanoparticle encapsulated FAM-labeled pre-miR-control for 24 hours. Cells were harvested and sorted by FACS. (**d**) Delivery of miR-107 expression in HNSCC cells. HNSCC cells were untreated or treated with 30 nmol/l of free pre-miR-control, free pre-miR-107, NP/pre-miR-control, or NP/pre-miR-107 for 24 hours. qPCR analysis of mature miR-107 was performed using a validated TaqMan assay. Data is presented and mean ± SEM. *$P < 0.001$, $n = 3$. HNSCC, head and neck squamous cell carcinoma; NP, nanoparticle; qPCR, quantitative PCR.

SCC25 cells, 148.2 for CAL27 cells, and 220.4 for UMSCC74A cells treated with NP/FAM-pre-miR-control. As shown in **Figure 1d**, a dramatic increase ($P < 0.001$) in mature miR-107 was detected in CAL27 and UMSCC74A cells after treatment with nanoparticle-encapsulated pre-miR-107 (NP/pre-miR-107; 30 nmol/l for 24 hours) compared to free pre-miR-107 (30 nmol/l for 24 hours) or nanoparticle encapsulated pre-miR-control (NP/pre-miR-control; 30 nmol/l for 24 hours). These results demonstrate that pre-miR-107 that is delivered into HNSCC cells is processed by Dicer to form the mature and functional miR-107.

NP/pre-miR-107 reduces the levels of miR-107 target genes

Our previous report identified PKCε as a novel target for miR-107 and also confirmed HIF1-β and CDK6 as miR-107-regulated genes in HNSCC.[11] Consistent with our published data, NP/pre-miR-107 treatment resulted in a decrease in PKCε, HIF1-β, and CDK6 mRNA expression and protein levels in CAL27 and UMSCC74A cells (**Figure 2a,b**). Moreover, phosphorylation of Akt (Ser^{473}), a downstream PKCε substrate, was reduced following NP/pre-miR-107 treatment. These results confirm that the lipid-based nanoparticles are an effective approach to deliver sufficient pre-miR-107 into HNSCC cells to modulate miR-107-regulated genes.

NP/pre-miR-107 inhibits clonogenic survival, cell invasion, and cell migration

CAL27 and UMSCC74A cells were incubated with NP/pre-miR-control or NP/pre-miR-107 (30 nmol/l) for 24 hours. Subsequently, cells were trypsinized and replated in appropriate experimental wells to assess for functional changes. Clonogenic survival assay was used to assess the clonal proliferation of surviving cells. Cell invasion was assessed using the modified Boyden chamber assay and cell migration was determined using the wound-healing assay. Clonogenic survival of CAL27 and UMSCC74A cells was compromised with NP/pre-miR-107 treatment; 44.2 ± 3.0% ($P < 0.005$) inhibition for CAL27 and 54.3 ± 2.4% inhibition for UMSCC74A ($P < 0.005$). In **Figure 3b,c**, CAL27 and UMSCC74A cells treated with NP/pre-miR-107 were significantly less invasive and motile than NP/pre-miR-control–treated cells. NP/miR-107 inhibited cell invasion by 84.6 ± 1.3% ($P < 0.001$) and 87.5 ± 1.1% ($P < 0.001$) in CAL27 and UMSCC74A, respectively. Cell migration was suppressed by 83.9 ± 4.0% ($P < 0.001$) in CAL27 cells and 64.6 ± 3.1% ($P < 0.001$) in UMSCC74A cells.

NP/pre-miR-107 reduces cancer-initiating cell population

A recent study reported that Nanog, a core embryonic stem cell (ESC) transcription factor, is regulated by PKCε.[12] Nanog expression was demonstrated to be enriched in cancer-initiating cells (CICs) suggesting that Nanog may play a critical role in maintaining

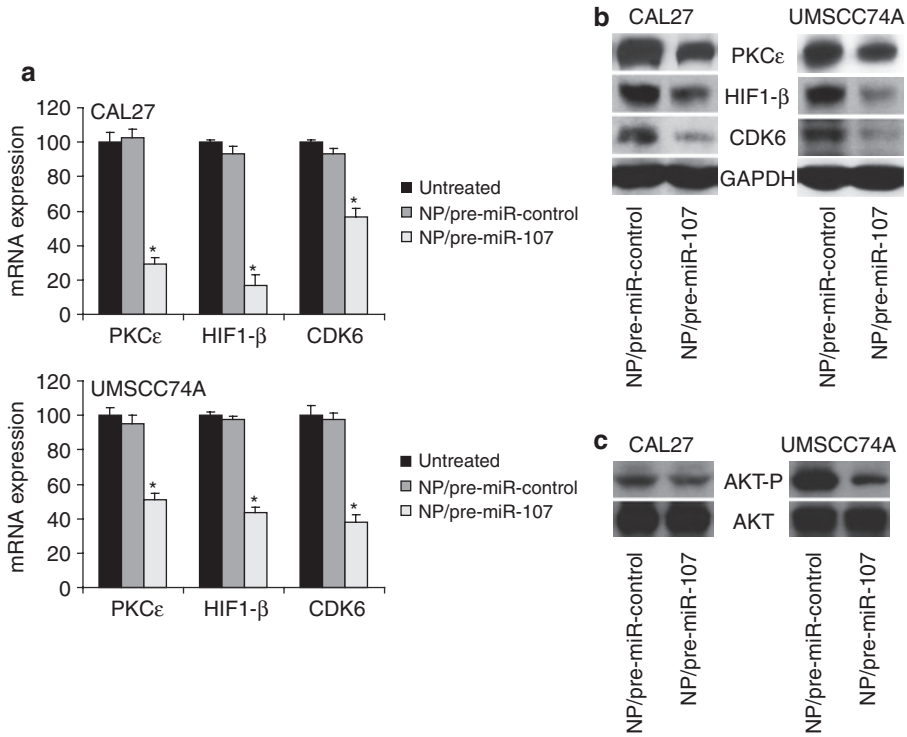

Figure 2 NP/pre-miR-107 targets miR-107 regulated genes. (**a**) mRNA expression of miR-107 target genes. CAL27 and UMSCC74A cells were untreated or treated with NP/pre-miR-control or NP/pre-miR-107 (30 nmol/l for 24 hours). Total mRNA was isolated and determined for PKCε, HIF1-β, and CDK6 by qPCR analysis. Data is presented and mean ± SEM. *$P < 0.001$, $n = 3$. (**b**) Protein levels of miR-107 target genes. CAL27 and UMSCC74A cells were untreated or treated with NP/pre-miR-control or NP/pre-miR-107 (30 nmol/l for 72 hours). Whole cell lysates were extracted and western blot analysis was performed using anti-PKCε, anti-HIF1-β, anti-CDK6, and anti-GAPDH antibodies. (**c**) Levels of active Akt. CAL27 and UMSCC74A cells were untreated or treated with NP/pre-miR-control or NP/pre-miR-107 (30 nmol/l for 72 hours). Whole cell lysates were extracted and western blot analysis was performed using anti-phospho-Akt and anti-Akt antibodies. CDK6, cyclin-dependent kinase 6; GAPDH, glyceraldehyde 3-phosphate dehydrogenase; HIF1-β, hypoxia-inducible factor 1-β; mRNA, messenger RNA; PKCε, protein kinase Cε; qPCR, quantitative PCR.

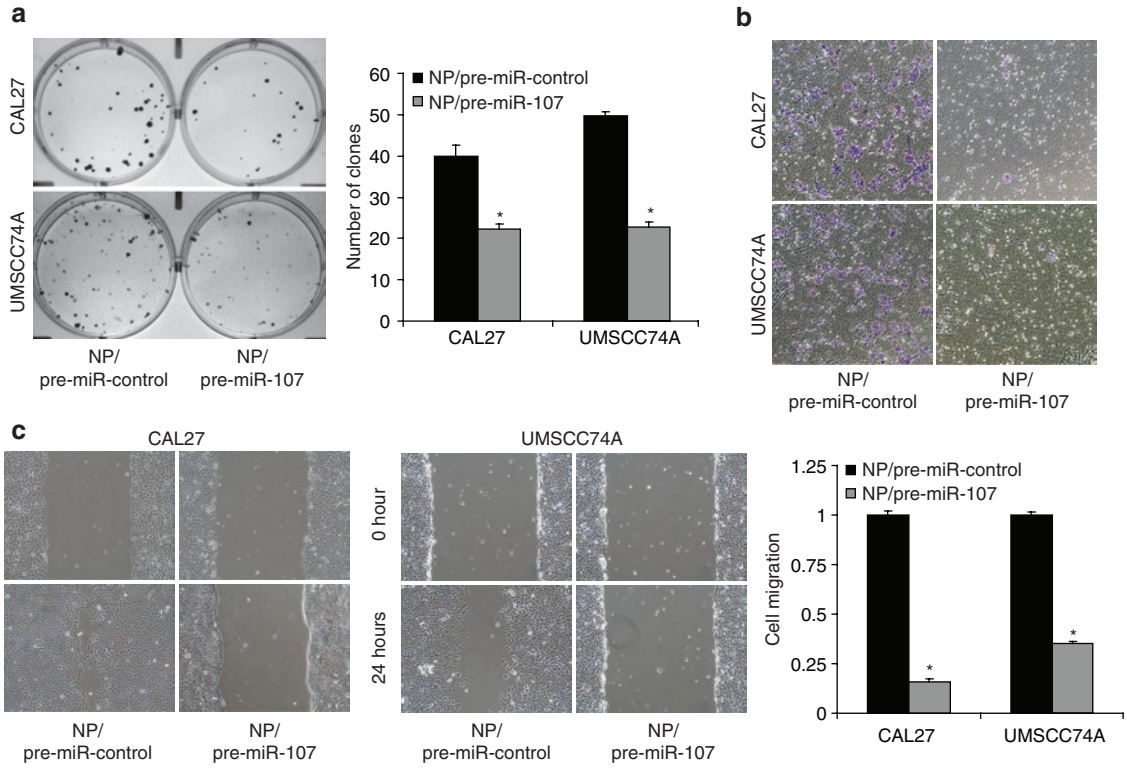

Figure 3 NP/pre-miR-107 inhibits clonogenic survival, cell invasion, and cell migration. (**a**) Clonogenic survival. Colonies were stained with crystal violet and counted. Data is presented and mean ± SEM. *$P < 0.005$, $n = 3$. (**b**) Cell invasion. Cell invasion was assessed using the modified Boyden chamber invasion assay with Matrigel basement membrane. (**c**) Cell migration. Cell migration was assessed using the wound-healing assay. Data is presented and mean ± SEM. *$P < 0.001$, $n = 3$.

the CIC phenotype.[13] Since PKCε is a validated target of miR-107, we determined whether CICs are modulated with NP/pre-miR-107 treatment. The ability of cells to form spheres under nonadherent culture conditions has been widely used as a functional *in vitro* assay to assess normal stem cells and CICs.[14–16] In comparison to NP/pre-miR-control treatment, NP/pre-miR-107 decreased tumorsphere formation efficiency from 7.4 ± 0.2 to 5.0 ± 0.2% in CAL27 and 1.9 ± 0.1 to 0.3 ± 0.1% in UMSCC74A (**Figure 4a**). Exposure to NP/pre-miR-107 reduced tumorsphere formation efficiency by 33 ± 2.7% ($P < 0.01$) and 84.2 ± 5.3% ($P < 0.01$) in CAL27 and UMSCC74A, respectively. In addition, NP/pre-miR-107 reduced tumorsphere diameter by 15.9 ± 0.5% ($P < 0.05$, $n = 6$) in CAL27 cells and 42.2 ± 6.1% ($P < 0.05$, $n = 4$) in UMSCC74A cells. In **Figure 4b**, mRNA expression of the three core ESC transcription factors, Nanog, Oct3/4, and Sox2, was markedly suppressed by 39–79% ($P < 0.01$) in CAL27 and UMSCC74A cells following NP/pre-miR-107 therapy. Ectopic overexpression of Nanog was sufficient to completely restore NP/pre-miR-107–mediated reduction in Oct3/4 (99% rescue) and Sox2 (151% rescue) (**Figure 4c**). More importantly, Nanog almost completely rescued the CIC number and size defect mediated by NP/pre-miR-107 providing further evidence that Nanog plays a critical role in CIC maintenance in HNSCC.

NP/pre-miR-107 retards the *in vivo* tumorigenicity of HNSCC cells

The antitumor efficacy of NP/pre-miR-107 was assessed in a xenograft model of HNSCC. CAL27 cells (1×10^6) were implanted into the flank of 8-week-old athymic nude mice and tumors were allowed to develop without treatment. At 2 weeks after implantation, mice with established tumors were randomly assigned to two treatment groups, NP/pre-miR-control (1 nmol, intravenous injection, twice weekly, $n = 7$) or NP/pre-miR-107 (1 nmol, intravenous injection, twice weekly, $n = 7$). As shown in **Figure 5a**, at the end of the treatment protocol, mice treated with NP/pre-miR-107 had significantly smaller tumors than mice treated with NP/pre-miR-control (45.2% inhibition, $P < 0.005$). Mean tumor volume increased by 670 ± 60% in NP/pre-miR-control–treated mice but only increased by 310 ± 50% in NP/pre-miR-107–treated mice. Kaplan–Meier analysis demonstrate that mice treated with NP/pre-miR-107 has a survival advantage over mice treated with NP/pre-miR-control ($P = 0.017$, $n = 7$). At the end of the treatment protocol, tumors were resected and assessed for expression of miR-107 and miR-107–targeted genes. Tumors from NP/pre-miR-107–treated mice had an approximately threefold increase ($P < 0.01$) in miR-107 expression compared to tumors from NP/pre-miR-control–treated mice (**Figure 5c**). Moreover, intratumoral expression of PKCε, HIF1-β, CDK6, Nanog, Sox2, and Oct3/4 was reduced by 45–75% ($P < 0.01$) following NP/pre-miR-107 treatment (**Figure 5d**).

Next, we determined the distribution efficiency of the cationic lipid-based nanoparticles to delivery therapeutic miRs *in vivo*. Athymic nude mice with established CAL27 xenografts were treated systemically with untagged (NP/pre-miR-control) or fluorescent-tagged (NP/FAM-labeled pre-miR-control) pre-miR-

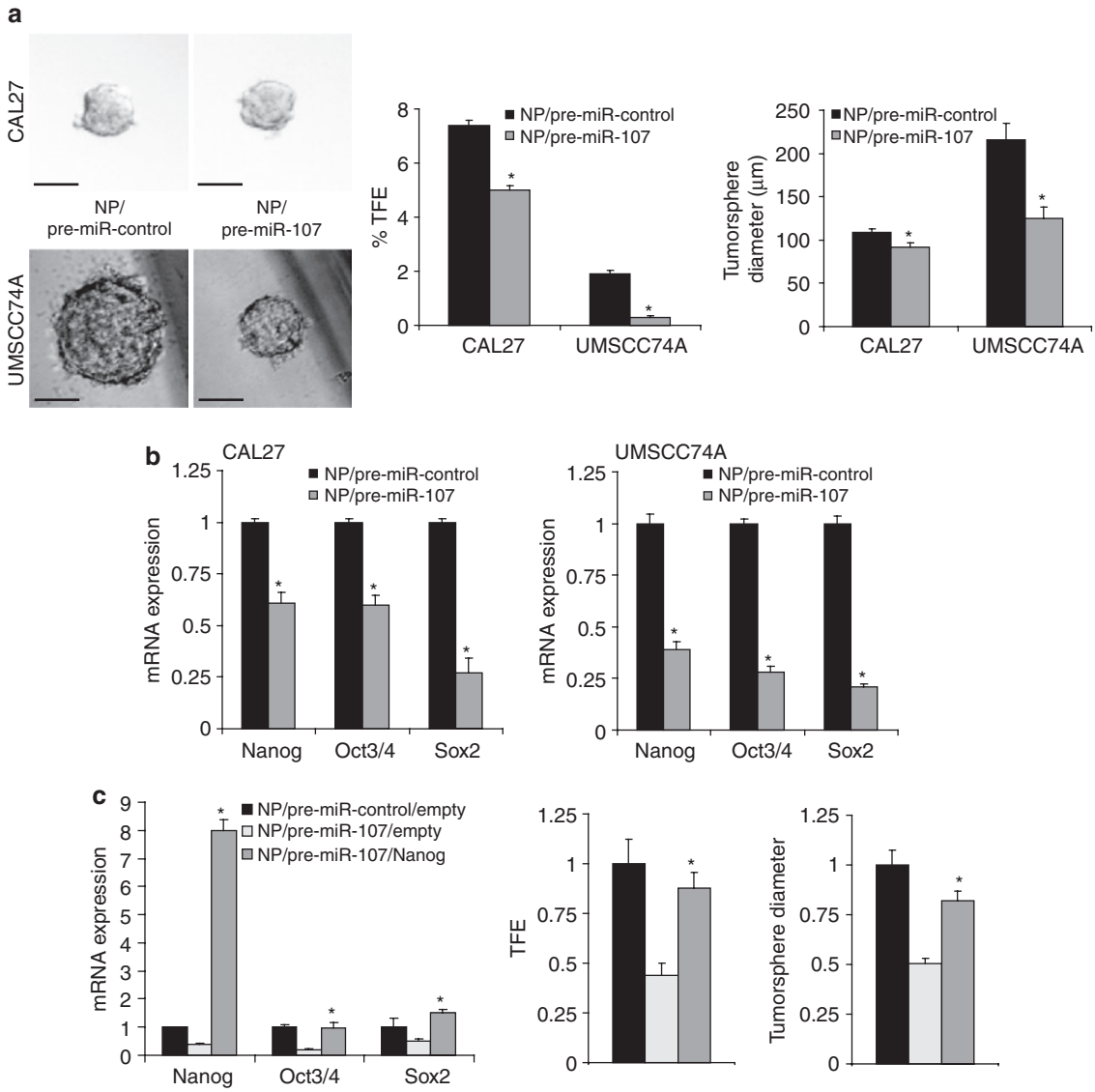

Figure 4 NP/pre-mir-107 reduces the cancer-initiating cell population. (**a**) Tumorspheres. CAL27 and UMSCC74A cells were treated with NP/pre-miR-control or NP/pre-miR-107 (30 nmol/l for 24 hours). Cells were harvested and seeded on low-attachment plates in a defined, serum-free culture medium at a density of 300 cells/well. Tumorspheres were allowed to grow for 7 days. Bar = 100 μm. Tumorsphere formation efficiency was calculated as the number of tumorspheres formed divided by the original number of cells seeded. Data is presented as mean ± SEM. *$P < 0.01$, $n = 6$. Tumorsphere diameter was measured using NIS-Elements software. Data is presented as mean ± SEM. *$P < 0.05$. (**b**) Expression of embryonic stem cell transcription factors. CAL27 and UMSCC74A cells were untreated or treated with NP/pre-miR-control or NP/pre-miR-107 (30 nmol/l for 24 hours). Total mRNA was isolated and determined for Nanog, Oct3/4, and Sox2 by qPCR analysis. Data is presented as mean ± SEM. *$P < 0.005$, $n = 3$. (**c**) Ectopic overexpression of Nanog rescues NP/pre-miR-107–mediated defect in CIC number and size. UMSCC74A cells were treated with NP/pre-miR-control or NP/pre-miR-107 (30 nmol/l for 24 hours) and subsequently transduced with pLenti6.2/empty or pLenti6.2/Nanog. Total mRNA was isolated and determined for Nanog, Oct3/4, and Sox2 by qPCR analysis. Data is presented as mean ± SEM. *$P < 0.005$, $n = 3$. Tumorsphere formation efficiency was calculated as the number of tumorspheres formed divided by the original number of cells seeded. *$P < 0.01$, $n = 6$. Tumorsphere diameter was measured using NIS-Elements software. *$P < 0.05$, $n = 6$. CIC, cancer-initiating cells; mRNA, messenger RNA; qPCR, quantitative PCR; TFE, tumorsphere formation efficiency.

control. After two treatments, tumors were resected and assessed for tumor distribution using confocal fluorescence microscopy. As shown in **Figure 5e**, fluorescence was undetectable in tumor sections from NP/pre-miR-control–treated mice. In contrast, fluorescence was readily detected in the cytosol of a majority of tumor cells from NP/FAM-labeled pre-miR-control–treated mice. Fluorescence intensity varied between tumor cells; some tumor cells exhibited weak fluorescence while other tumor cells exhibited strong fluorescence. These results indicate that cationic nanoparticles were widely distributed in the tumor and an efficient approach to systemically deliver miRs *in vivo*.

DISCUSSION

Our laboratory and others demonstrated that miR-107 functions as a tumor suppressor in various cancers by controlling the levels of PKCε, HIF1-β, and CDK6. Restoration of miR-107 inhibits HIF1-β levels and retards tumor growth in HCT116 colon cancer cells.[17] In pancreatic cancer cells, MiaPACA-2 and PANC-1,

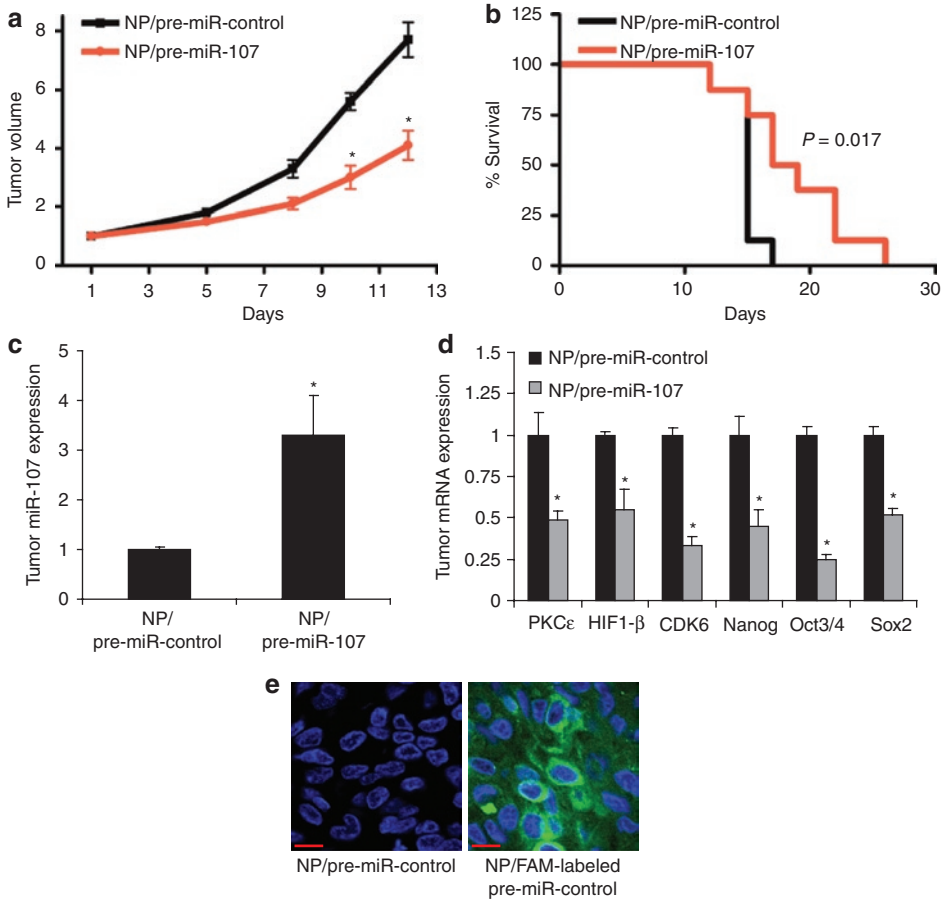

Figure 5 NP/pre-miR-107 suppresses the *in vivo* tumorigenicity of HNSCC cells. (**a**) Tumor growth. CAL27 cells were implanted into the flanks of 8-week-old female athymic nude mice and tumors were allowed to develop without treatment. At 2 weeks after implantation, mice with palpable tumors were assigned to two experimental groups and treated with NP/pre-miR-control or NP/pre-miR-107 (1 nmol, twice weekly, $n = 7$) by intravenous injection through the tail vein. Tumors were measured using a digital caliper and tumor volumes were calculated. Data is presented and mean ± SEM. *$P < 0.005$. (**b**) Overall survival. Kaplan–Meier analysis was performed between the NP/pre-miR-control and the NP/pre-miR-107 group. $P = 0.017$, $n = 7$. (**c**) Tumor expression of miR-107. (**d**) Tumor expression of miR-107-mediated genes. Tumors from NP/pre-miR-control- and NP/pre-miR-107–treated mice were resected at the end of the treatment protocol. Total mRNA was isolated and determined for mature miR-107, PKCε, HIF1-β, CDK6, Nanog, Oct3/4, and Sox2 expression by qPCR analysis. Data is presented as mean ± SEM. *$P < 0.01$. (**e**) Tumor distribution of pre-miR using the cationic lipid-based nanoparticles. CAL27 cells were implanted into the flanks of 8-week-old female athymic nude mice and tumors were allowed to develop without treatment. At 2 weeks after implantation, tumor-bearing mice were treated with NP/pre-miR-control or NP/FAM-labeled pre-miR-control (1 nmol, intravenous injection, twice over 5-day period). Tumors were resected, sectioned, mounted with ProLong Gold Antifade reagent with DAPI (Invitrogen, Carlsbad, CA), and visualized for tumor distribution using confocal fluorescence microscopy. A representative tumor section from a NP/pre-miR-control- or NP/FAM-labeled pre-miR-control–treated mouse is presented. Bar = 10 µm. CDK6, cyclin-dependent kinase 6; DAPI, 4′,6-diamidino-2-phenylindole; HIF1-β, hypoxia inducible factor 1-β; HNSCC, head and neck squamous cell carcinoma; mRNA, messenger RNA; PKCε, protein kinase Cε; qPCR, quantitative PCR.

miR-107 repressed CDK6 levels and inhibited cell proliferation.[18] Similarly, miR-107 was reported to target CDK6 and inhibit cell proliferation in gastric cancer cells.[19] Recent work from our laboratory showed that miR-107 expression is significantly reduced in primary HNSCC tumors compared to matched adjacent normal epithelium.[11] We identified PKCε as a novel miR-107 target and validated HIF1-β and CDK6 as miR-107 targets in HNSCC.[11] Moreover, stable overexpression of miR-107 is sufficient to dramatically retard the tumor growth of CAL27 HNSCC cells in athymic nude mice.[11] Taken together, these studies provide evidence that miR-107 may be a potential anticancer therapeutic for several cancers, including HNSCC.

There are several challenges associated with the application of miRs as therapeutic agents. miRs are rapidly degraded in circulation and have poor membrane penetration due to its negative charge. To overcome these obstacles, several strategies have been developed to restore the levels of tumor suppressor miRs *in vivo*. Systemic administration of miR-26a using an adeno-associated virus suppressed tumorigenicity in the Tet-o-MYC/LAP-tTA transgenic model of hepatocellular carcinoma.[20] Delivery of miR-34a using liposome-polycation-hyaluronic acid nanoparticles decreased survivin expression and demonstrated anticancer efficacy in the B16F10 lung metastasis mouse model.[21] A recent study demonstrated that polyethylenimine-mediated delivery of miR-134 inhibited the *in vivo* tumor growth of colon cancer cell.[22] In this study, cationic lipid-based nanoparticle encapsulation dramatically enhanced the delivery of pre-miR-107 into HNSCC cells resulting in downregulation of miR-107–targeted genes, PKCε, HIF1-β, and CDK6. Importantly, systemic treatment of NP/pre-miR-107 showed significant efficacy in a preclinical mouse

model of HNSCC to reduce tumor growth and prolong survival. Our results indicate that cationic lipid-based nanoparticles are amendable to efficiently deliver miRs to HNSCC cells *in vitro* and *in vivo*.

Development of lipid-based nanoparticles as a carrier to deliver standard chemotherapeutics has gained traction since the Food and Drug Administration approval of caelyx, a liposome-based formulation of doxorubicin, for breast cancer. A number of lipid-based nanoparticle formulations of approved chemotherapeutics, including cis-platinum, docetaxel, and vincristine, were studied in early to late stage clinical trials.[23–26] In addition to chemotherapeutics, various lipid-based nanoparticle formulations were reported to be efficient carrier systems to deliver oligonucleotides, small interfering RNAs, and miRNAs *in vivo*.[27,28] Delivery of c-*myc* antisense oligonucleotides using disialoganglioside GD2-targeted cationic liposomes reduced tumor growth and enhanced survival in a mouse model of melanoma.[29] Encapsulation of bcl-2 antisense oligonucleotides with transferrin receptor-targeted lipid nanoparticles resulted in superior antitumor efficacy compared to free bcl-2 antisense oligonucleotides.[30] c-Met small interfering RNA-encapsulated nanoparticles suppressed tumor growth in an orthotopic U-87MG glioblastoma model with minimal systemic toxicity.[31] High-density lipoprotein nanoparticles were shown to efficiently deliver small interfering RNA targeting signal transducer and activator of transcription 3 (STAT3) and focal adhesion kinase (FAK) to block tumor growth and metastasis in orthotopic mouse models of ovarian cancer.[32] Our work and these published studies demonstrate that lipid-based nanoparticles are an effective carrier system to deliver different classes of anticancer therapeutics *in vivo*.

PKCε is a well-recognized oncogene that promotes various aspects of tumorigenesis by controlling apoptosis and cell invasion, migration, and survival. PKCε-mediated phosphorylation of vimentin regulates integrin recycling to enhance cell migration.[33] RhoA and RhoC, regulators of cell invasion and migration, are directly phosphorylated by PKCε resulting in an increase in RhoA and RhoC activation in HNSCC.[34] PKCε enhances Bad phosphorylation to protect LnCaP prostate cancer cells from apoptotic stimuli.[35] In glioma cells, PKCε modulates apoptosis and survival through regulation of Akt.[36] PKCε was shown to directly phosphorylate Akt at Ser^{473} leading to a full Akt activation state.[37] Consistent with this model of Akt activation, levels of phospho-Akt (Ser^{473}) was reduced in CAL27 and UMSCC74A cells following treatment with NP/pre-miR-107. This observation indicates that an adequate amount of pre-miR-107 can be delivered into HNSCC cells to block the PKCε signaling cascade.

HIF-1, a transcription factor composed of a heterodimer complex of HIF-1α and HIF-1β, regulates the transcription of a cadre of genes involved in angiogenesis, apoptosis, and metastasis. HIF-1 was reported to regulate matrix metalloproteinases (MMPs), MMP2 and MMP9, and lysyl oxidase to modulate tumor cell migration and/or invasion. MMP2 and MMP9 are endopeptidases responsible for degradation of extracellular matrix to facilitate tumor invasion. Lysyl oxidase increases cell migration through enhanced cell–matrix adhesion and focal adhesion kinase activity.[38] Hypoxia-mediated invasion was attenuated with genetic ablation of lysyl oxidase in numerous cancer cell lines, including HNSCC cells.[38] Interestingly, a recent study demonstrated that lysyl oxidase increases HIF-1 activity through a phosphoinositide 3-kinase (PI3K)-Akt pathway.[39] This finding suggests that PKCε through Akt activation may be able to enhance the HIF-1-lysyl oxidase positive feedback loop signal. Thus, the coordinated downregulation of PKCε and HIF-1β by miR-107 may act in concert to dampen the invasive and motile potential of HNSCC cells.

CICs are a limited population of tumors cells with the unique capacity to self-renew to expand the CIC pool and to differentiate into hetergeneous cells that form the bulk of the tumor. Evidence has accumulated to support the existence of CICs in HNSCC.[40–42] Nanog, Oct4, and Sox2 are transcription factors well-recognized as critical players in ESC maintenance and self-renewal.[43–46] The role of these transcription factors in CICs is beginning to emerge. Nanog and Oct3/4 were reported to be highly expressed in tumorspheres cultivated from HNSCC cell lines.[13] In support, a recent study showed that tumorspheres isolated from several established HNSCC cell lines have enhanced expression of Nanog, Oct3/4, and Sox2.[47] Our results showed that NP/pre-miR-107 treatment results in a decrease in tumorsphere formation efficiency and size. Moreover, the expression of Nanog, Oct3/4, and Sox2 were decreased in CAL27 and UMSCC74A cells treated with NP/pre-miR-107. Overexpression of Nanog was sufficient to restore NP/pre-miR-107–mediated decrease in Oct3/4 and Sox2 expression and reduction in CIC number and size indicating that Nanog may function as the signaling hub in the ESC transcription factor circuitry to control CICs. It is unclear, at this time, how miR-107 regulates Nanog expression in HNSCC. PKCε was shown to mediate Nanog phosphorylation and nuclear translocation to control Nanog function.[12] Thus, a potential possibility is that the miR-107-PKCε-Nanog signaling axis may be involved in CIC maintenance in HNSCC.

In summary, cationic lipid-based nanoparticle delivery of pre-miR-107 suppresses the tumorigenesis of HNSCC *in vitro* and *in vivo*. Our results demonstrate the potential clinical application of nanoparticles as a carrier system to deliver therapeutic miRs.

MATERIALS AND METHODS

Cell culture. SCC15, SCC25, and CAL27 cells were obtained from American Type Culture Collection (Rockville, MD). UMSCC74A cells were obtained from Thomas Carey at the University of Michigan Medical School. SCC15 and SCC25 cells were grown in Dulbecco's modified Eagle's medium/F12 (1:1) medium containing 10% fetal bovine serum. CAL27 and UMSCC74A cells were cultured in Dulbecco's modified Eagle's medium medium containing 10% fetal bovine serum.

Cationic lipid nanoparticle preparation. Cationic lipid nanoparticles were prepared from DDAB (Sigma-Aldrich, St Louis, MO), cholesterol (Avanti Polar Lipids, Alabaster, AL) and TPGS (Eastman Chemical, Anglesey, UK) by ethanol dilution method. DDAB, cholesterol, and TPGS (molar ratio of 60:35:5) were dissolved in ethanol. Nanoparticles encapsulated with pre-miR-control or pre-miR-107 (Applied Biosystems, Foster City, CA) were prepared by mixing cationic lipid nanoparticles with pre-miR-control or pre-miR-107 at weight ratio of 10:1, incubated for 30 minutes at room temperature, and added into phosphate-buffered saline (PBS) solution (pH 7.4) upon stirring at room temperature. Ethanol was removed by dialysis using a molecular weight cut-off 10,000 Dalton Float-ALyser (Spectrum Laboratories, Ranco Dominguez, CA) and against PBS

(pH 7.4) for 24 hours at room temperature. The particle size of nanoparticles was analyzed on a NICOMP Particle Sizer model 370 (Particle Sizing Systems, Santa Barbara, CA). The volume-weighted Gaussian distribution analysis was used to determine the mean nanoparticle diameter. Zeta potential of the nanoparticles was determined on a ZetaPALS (Brookhaven Instruments, Worcestershire, NY).

Encapsulation efficiency. The encapsulation efficiency was determined by measuring the amount of extractable miR in the nanoparticles. NP/pre-miR-107 was lysed with 0.5% sodium dodecyl sulfate and 1% Triton X-100, and 100 µl of TE buffer was added. The mixture was incubated for 30 minutes at 37 °C. The samples were then further diluted with TE buffer, and the pre-miR-107 concentration was measured with the RiboGreen RNA reagent (Invitrogen, Carlsbad, CA) using a plate reader at an excitation wavelength of 485 nm and an emission wavelength of 520 nm. Each sample was assayed in triplicate. The pre-miR-107 encapsulation efficiency was calculated using the following formula: encapsulation efficiency (%) = (actual pre-miR-107 loading/theoretical pre-miR-107 loading) × 100

TEM. TEM images of NP/pre-miR-107 were acquired using JEOL 100CX II TEM (JEOL, Tokyo, Japan). Briefly, 5 µl of NP-pre-miR-107 was dropped onto a 300 mesh carbon coated copper grid (Ted Pella, Redding, CA). Excess sample was removed by blotting with a filter paper. The grid was air-dried and viewed in TEM without staining.

Flow cytometry. CAL27, SCC15, SCC25, and SCC74A cells were untreated or treated with 30 nmol/l of free or nanoparticle-encapsulated FAM-labeled-pre-miR-control. After 24 hours, the cells were washed with PBS (pH 7.4) and then harvested with 0.05% trypsin/0.025% EDTA. Detached cells were washed, resuspended in PBS, and analyzed on a FACSVantage flow cytometer (BD Biosciences, Franklin Lakes, NJ) at the Ohio State University Comprehensive Cancer Center Analytical Cytometry Core.

Quantitative reverse transcription PCR. Real-time reverse transcription PCR was performed using Real-time PCR Universal Reagent and ABI-7900HT real-time PCR machine (Applied Biosystems). All reactions were done in a 20 µl reaction volume in triplicate using validated TaqMan Gene Expression Assays for mature miR-107, RNU44, Nanog, Oct3/4, Sox2, PKCε, HIF1-β, CDK6, and GAPDH. PCR amplification consisted of an initial denaturation step at 95 °C for 10 minutes, followed by 40 cycles of PCR at 95 °C for 15 seconds, 60 °C for 60 seconds. Standard curves were generated and the relative amount of mature miR-107 and Nanog, Oct3/4, Sox2, PKCε, HIF1-β, and CDK6 was normalized to RNU44 and GAPDH, respectively.

Western blot analysis. Whole cell lysates were mixed with Laemmli loading buffer, boiled, separated by sodium dodecyl sulfate polyacrylamide gel electrophoresis, and transferred to a nitrocellulose membrane. Subsequently, immunoblot analyses were performed using antibodies specific to PKCε (Santa Cruz Biotechnology, Santa Cruz, CA), CDK6 (Thermo Fisher Scientific, Waltham, MA), HIF1-β, phospho-Akt, Akt, or GADPH (Cell Signaling Technology, Danvers, MA). The signal was developed with ECL (Thermo Fisher Scientific) after incubation with appropriate secondary antibodies.

Cell invasion and migration. Cell invasion was determined using the BD Biocoat Matrigel Invasion Chamber (BD Biosciences). HNSCC cells were incubated with NP/pre-miR-control or NP/pre-miR-107 for 24 hours (30 nmol/l), harvested and resuspended in serum-free Dulbecco's modified Eagle's medium medium. An aliquot (4×10^4 cells) of the prepared cell suspension was carefully added into the chamber and incubated for 24 hours at 37 °C. The non-invaded cells were carefully removed from the interior of the inserts with a cotton-tipped swab. The inserts were then stained with 0.25% crystal violet in 25% methanol, washed, and air-dried. Cell migration was determined using the wound-healing assay. Confluent monolayer cells were scratched with a pipette tip, rinsed with PBS, and fresh culture media were added. Wounds areas were marked and photographed at different time points using a phase-contrast microscope.

Clonogenic survival. HNSCC cells were incubated with NP/pre-miR-control or NP/pre-miR-107 for 24 hours (30 nmol/l), harvested, and resuspended in complete growth media. Cells were seeded onto 6-well plates and allowed to grow until visible colonies formed (7 days). Cell colonies were fixed with cold methanol, stained with 0.25% crystal violet in 25% methanol, washed and air-dried.

Tumorsphere formation efficiency. HNSCC cells were incubated with NP/pre-miR-control or NP/pre-miR-107 for 24 hours (30 nmol/l). Cells were harvested and seeded in a serum-free defined medium consisting of keratinocyte serum-free medium supplemented with epidermal growth factor, basic fibroblast growth factor, insulin, and hydrocortisone in low-attachment plates (Corning, Corning, NY) for tumorspheres. Tumorsphere formation efficiency was calculated as the number of tumorspheres formed in 7 days divided by the initial number of single cells seeded.

In vivo *efficacy of NP/pre-miR-107 in a HNSCC xenograft model.* CAL27 cells (1×10^6) mixed with Matrigel (1:1) were implanted into the flanks of 8-week-old female athymic nude mice (National Cancer Institute, Frederick, MD) and tumors were allowed to develop without treatment. At 2 weeks after implantation, mice with palpable tumors were assigned to two experimental groups and treated with NP/pre-miR-control or NP/pre-miR-107 (1 nmol, twice weekly, $n = 7$) by intravenous injection through the tail vein. Tumors were measured using a digital caliper and tumor volumes were calculated using the formula: tumor volume = length × width × height × 0.5. Any mouse with a tumor volume equal to or greater than 1,000 mm^3 was euthanized and removed from the study. All animal work performed was in accordance with and approved by the Institutional Animal Care and Use Committee at the Ohio State University.

Distribution of NP/FAM-labeled pre-miR in a HNSCC xenograft model. CAL27 cells (1×10^6) mixed with Matrigel (1:1) were implanted into the flanks of 8-week-old female athymic nude mice (National Cancer Institute) and tumors were allowed to develop without treatment. Mice with tumors (200–250 mm^3) were assigned to two experimental groups and treated with NP/pre-miR-control or NP/FAM-labeled pre-miR (1 nmol, intravenous injection, twice over 5-day period) by intravenous injection through the tail vein. After two treatments, tumors were resected, sectioned, mounted with ProLong Gold Antifade reagent with DAPI (Invitrogen), and visualized for tumor distribution of FAM-labeled pre-miR-control using confocal fluorescence microscopy with a Zeiss LSM-510 microscope (Carl Zeiss, Thornwood, NY).

ACKNOWLEDGMENTS

This work was supported in part by the National Cancer Institute at the National Institutes of Health (R01CA135096); The Michelle Theado Memorial Grant from the Joan Bisesi Fund for Head and Neck Oncology Research; and Arthur G. James Cancer Hospital and Richard J. Solove Research Institute, The Ohio State University Comprehensive Cancer Center. The authors declared no conflict of interest.

REFERENCES

1. Kamangar, F, Dores, GM and Anderson, WF (2006). Patterns of cancer incidence, mortality, and prevalence across five continents: defining priorities to reduce cancer disparities in different geographic regions of the world. *J Clin Oncol* **24**: 2137–2150.
2. Leemans, CR, Braakhuis, BJ and Brakenhoff, RH (2011). The molecular biology of head and neck cancer. *Nat Rev Cancer* **11**: 9–22.
3. Filipowicz, W, Bhattacharyya, SN and Sonenberg, N (2008). Mechanisms of post-transcriptional regulation by microRNAs: are the answers in sight? *Nat Rev Genet* **9**: 102–114.
4. Avissar, M, Christensen, BC, Kelsey, KT and Marsit, CJ (2009). MicroRNA expression ratio is predictive of head and neck squamous cell carcinoma. *Clin Cancer Res* **15**: 2850–2855.
5. Calin, GA and Croce, CM (2006). MicroRNA signatures in human cancers. *Nat Rev Cancer* **6**: 857–866.
6. Croce, CM (2009). Causes and consequences of microRNA dysregulation in cancer. *Nat Rev Genet* **10**: 704–714.
7. Hwang, HW and Mendell, JT (2006). MicroRNAs in cell proliferation, cell death, and tumorigenesis. *Br J Cancer* **94**: 776–780.

8. Lu, J, Getz, G, Miska, EA, Alvarez-Saavedra, E, Lamb, J, Peck, D *et al.* (2005). MicroRNA expression profiles classify human cancers. *Nature* **435**: 834–838.
9. Wong, TS, Liu, XB, Wong, BY, Ng, RW, Yuen, AP and Wei, WI (2008). Mature miR-184 as Potential Oncogenic microRNA of Squamous Cell Carcinoma of Tongue. *Clin Cancer Res* **14**: 2588–2592.
10. Kozaki, K, Imoto, I, Mogi, S, Omura, K and Inazawa, J (2008). Exploration of tumor-suppressive microRNAs silenced by DNA hypermethylation in oral cancer. *Cancer Res* **68**: 2094–2105.
11. Datta, J, Smith, A, Lang, JC, Islam, M, Dutt, D, Teknos, TN *et al.* (2011). microRNA-107 functions as a candidate tumor-suppressor gene in head and neck squamous cell carcinoma by downregulation of protein kinase Cε *Oncogene* (epub ahead of print) (doi:10.1038/onc.2011.565).
12. Bourguignon, LY, Spevak, CC, Wong, G, Xia, W and Gilad, E (2009). Hyaluronan-CD44 interaction with protein kinase C(epsilon) promotes oncogenic signaling by the stem cell marker Nanog and the Production of microRNA-21, leading to down-regulation of the tumor suppressor protein PDCD4, anti-apoptosis, and chemotherapy resistance in breast tumor cells. *J Biol Chem* **284**: 26533–26546.
13. Chiou, SH, Yu, CC, Huang, CY, Lin, SC, Liu, CJ, Tsai, TH *et al.* (2008). Positive correlations of Oct-4 and Nanog in oral cancer stem-like cells and high-grade oral squamous cell carcinoma. *Clin Cancer Res* **14**: 4085–4095.
14. Yu, F, Yao, H, Zhu, P, Zhang, X, Pan, Q, Gong, C *et al.* (2007). let-7 regulates self renewal and tumorigenicity of breast cancer cells. *Cell* **131**: 1109–1123.
15. Liu, S, Dontu, G, Mantle, ID, Patel, S, Ahn, NS, Jackson, KW *et al.* (2006). Hedgehog signaling and Bmi-1 regulate self-renewal of normal and malignant human mammary stem cells. *Cancer Res* **66**: 6063–6071.
16. Dontu, G, Abdallah, WM, Foley, JM, Jackson, KW, Clarke, MF, Kawamura, MJ *et al.* (2003). *In vitro* propagation and transcriptional profiling of human mammary stem/progenitor cells. *Genes Dev* **17**: 1253–1270.
17. Yamakuchi, M, Lotterman, CD, Bao, C, Hruban, RH, Karim, B, Mendell, JT *et al.* (2010). P53-induced microRNA-107 inhibits HIF-1 and tumor angiogenesis. *Proc Natl Acad Sci USA* **107**: 6334–6339.
18. Lee, KH, Lotterman, C, Karikari, C, Omura, N, Feldmann, G, Habbe, N *et al.* (2009). Epigenetic silencing of MicroRNA miR-107 regulates cyclin-dependent kinase 6 expression in pancreatic cancer. *Pancreatology* **9**: 293–301.
19. Feng, L, Xie, Y, Zhang, H and Wu, Y (2011). miR-107 targets cyclin-dependent kinase 6 expression, induces cell cycle G1 arrest and inhibits invasion in gastric cancer cells. *Med Oncol* (epub ahead of print) (doi:10.1007/s12032-011-9823-1).
20. Kota, J, Chivukula, RR, O'Donnell, KA, Wentzel, EA, Montgomery, CL, Hwang, HW *et al.* (2009). Therapeutic microRNA delivery suppresses tumorigenesis in a murine liver cancer model. *Cell* **137**: 1005–1017.
21. Chen, Y, Zhu, X, Zhang, X, Liu, B and Huang, L (2010). Nanoparticles modified with tumor-targeting scFv deliver siRNA and miRNA for cancer therapy. *Mol Ther* **18**: 1650–1656.
22. Ibrahim, AF, Weirauch, U, Thomas, M, Grünweller, A, Hartmann, RK and Aigner, A (2011). MicroRNA replacement therapy for miR-145 and miR-33a is efficacious in a model of colon carcinoma. *Cancer Res* **71**: 5214–5224.
23. Mylonakis, N, Athanasiou, A, Ziras, N, Angel, J, Rapti, A, Lampaki, S *et al.* (2010). Phase II study of liposomal cisplatin (Lipoplatin) plus gemcitabine versus cisplatin plus gemcitabine as first line treatment in inoperable (stage IIIB/IV) non-small cell lung cancer. *Lung Cancer* **68**: 240–247.
24. Boulikas, T (2009). Clinical overview on Lipoplatin: a successful liposomal formulation of cisplatin. *Expert Opin Investig Drugs* **18**: 1197–1218.
25. Thomas, DA, Sarris, AH, Cortes, J, Faderl, S, O'Brien, S, Giles, FJ *et al.* (2006). Phase II study of sphingosomal vincristine in patients with recurrent or refractory adult acute lymphocytic leukemia. *Cancer* **106**: 120–127.
26. Immordino, ML, Brusa, P, Arpicco, S, Stella, B, Dosio, F and Cattel, L (2003). Preparation, characterization, cytotoxicity and pharmacokinetics of liposomes containing docetaxel. *J Control Release* **91**: 417–429.
27. Fenske, DB and Cullis, PR (2008). Liposomal nanomedicines. *Expert Opin Drug Deliv* **5**: 25–44.
28. Zhao, X, Pan, F, Holt, CM, Lewis, AL and Lu, JR (2009). Controlled delivery of antisense oligonucleotides: a brief review of current strategies. *Expert Opin Drug Deliv* **6**: 673–686.
29. Pastorino, F, Brignole, C, Marimpietri, D, Pagnan, G, Morando, A, Ribatti, D *et al.* (2003). Targeted liposomal c-myc antisense oligodeoxynucleotides induce apoptosis and inhibit tumor growth and metastases in human melanoma models. *Clin Cancer Res* **9**: 4595–4605.
30. Zhang, X, Koh, CG, Yu, B, Liu, S, Piao, L, Marcucci, G *et al.* (2009). Transferrin receptor targeted lipopolyplexes for delivery of antisense oligonucleotide g3139 in a murine k562 xenograft model. *Pharm Res* **26**: 1516–1524.
31. Jin, J, Bae, KH, Yang, H, Lee, SJ, Kim, H, Kim, Y *et al.* (2011). *In vivo* specific delivery of c-Met siRNA to glioblastoma using cationic solid lipid nanoparticles. *Bioconjug Chem* **22**: 2568–2572.
32. Shahzad, MM, Mangala, LS, Han, HD, Lu, C, Bottsford-Miller, J, Nishimura, M *et al.* (2011). Targeted delivery of small interfering RNA using reconstituted high-density lipoprotein nanoparticles. *Neoplasia* **13**: 309–319.
33. Ivaska, J, Vuoriluoto, K, Huovinen, T, Izawa, I, Inagaki, M and Parker, PJ (2005). PKCepsilon-mediated phosphorylation of vimentin controls integrin recycling and motility. *EMBO J* **24**: 3834–3845.
34. Pan, Q, Bao, LW, Teknos, TN and Merajver, SD (2006). Targeted disruption of protein kinase C epsilon reduces cell invasion and motility through inactivation of RhoA and RhoC GTPases in head and neck squamous cell carcinoma. *Cancer Res* **66**: 9379–9384.
35. Meshki, J, Caino, MC, von Burstin, VA, Griner, E and Kazanietz, MG (2010). Regulation of prostate cancer cell survival by protein kinase Cepsilon involves bad phosphorylation and modulation of the TNFalpha/JNK pathway. *J Biol Chem* **285**: 26033–26040.
36. Okhrimenko, H, Lu, W, Xiang, C, Hamburger, N, Kazimirsky, G and Brodie, C (2005). Protein kinase C-epsilon regulates the apoptosis and survival of glioma cells. *Cancer Res* **65**: 7301–7309.
37. Zhang, J, Baines, CP, Zong, C, Cardwell, EM, Wang, G, Vondriska, TM *et al.* (2005). Functional proteomic analysis of a three-tier PKCepsilon-Akt-eNOS signaling module in cardiac protection. *Am J Physiol Heart Circ Physiol* **288**: H954–H961.
38. Erler, JT, Bennewith, KL, Nicolau, M, Dornhöfer, N, Kong, C, Le, QT *et al.* (2006). Lysyl oxidase is essential for hypoxia-induced metastasis. *Nature* **440**: 1222–1226.
39. Pez, F, Dayan, F, Durivault, J, Kaniewski, B, Aimond, G, Le Provost, GS *et al.* (2011). The HIF-1-inducible lysyl oxidase activates HIF-1 via the Akt pathway in a positive regulation loop and synergizes with HIF-1 in promoting tumor cell growth. *Cancer Res* **71**: 1647–1657.
40. Prince, ME, Sivanandan, R, Kaczorowski, A, Wolf, GT, Kaplan, MJ, Dalerba, P *et al.* (2007). Identification of a subpopulation of cells with cancer stem cell properties in head and neck squamous cell carcinoma. *Proc Natl Acad Sci USA* **104**: 973–978.
41. Chen, YC, Chen, YW, Hsu, HS, Tseng, LM, Huang, PI, Lu, KH *et al.* (2009). Aldehyde dehydrogenase 1 is a putative marker for cancer stem cells in head and neck squamous cancer. *Biochem Biophys Res Commun* **385**: 307–313.
42. Clay, MR, Tabor, M, Owen, JH, Carey, TE, Bradford, CR, Wolf, GT *et al.* (2010). Single-marker identification of head and neck squamous cell carcinoma cancer stem cells with aldehyde dehydrogenase. *Head Neck* **32**: 1195–1201.
43. Niwa, H, Miyazaki, J and Smith, AG (2000). Quantitative expression of Oct-3/4 defines differentiation, dedifferentiation or self-renewal of ES cells. *Nat Genet* **24**: 372–376.
44. Mitsui, K, Tokuzawa, Y, Itoh, H, Segawa, K, Murakami, M, Takahashi, K *et al.* (2003). The homeoprotein Nanog is required for maintenance of pluripotency in mouse epiblast and ES cells. *Cell* **113**: 631–642.
45. Masui, S, Nakatake, Y, Toyooka, Y, Shimosato, D, Yagi, R, Takahashi, K *et al.* (2007). Pluripotency governed by Sox2 via regulation of Oct3/4 expression in mouse embryonic stem cells. *Nat Cell Biol* **9**: 625–635.
46. Torres, J and Watt, FM (2008). Nanog maintains pluripotency of mouse embryonic stem cells by inhibiting NFkappaB and cooperating with Stat3. *Nat Cell Biol* **10**: 194–201.
47. Chen, C, Wei, Y, Hummel, M, Hoffmann, TK, Gross, M, Kaufmann, AM *et al.* (2011). Evidence for epithelial-mesenchymal transition in cancer stem cells of head and neck squamous cell carcinoma. *PLoS ONE* **6**: e16466.